Model predictive control based virtual synchronous generator for parallel-connected three-phase split-source converters in islanded AC Microgrids

Abou-Hussein, Walaa M.; Dabour, Sherif; Hamad, Mostafa S.; Rashad, Essam M.

Published in:
Energy Reports

DOI:
10.1016/j.egyr.2022.12.075

Publication date:
2023

Document Version
Publisher's PDF, also known as Version of record

Energy Reports 9 (2023) 1696–1706

Contents lists available at ScienceDirect

Energy Reports

journal homepage: www.elsevier.com/locate/egyr

Research paper

Model predictive control based virtual synchronous generator for parallel-connected three-phase split-source converters in islanded AC Microgrids

Walaa M. Abou-Hussein [a,*], Sherif M. Dabour [b,c], Mostafa S. Hamad [d], Essam M. Rashad [b]

[a] Department of Mechatronics, Alexandria Higher Institute of Engineering & Technology (AIET), Alexandria, Egypt
[b] Department of Electrical Power and Machines Engineering, Tanta University, Tanta, Egypt
[c] Department of Electrical Power Engineering, School of Computing, Engineering, and Built Environment, Glasgow Caledonian University, Glasgow G4 0BA, UK
[d] Research and Development Center, Arab Academy for Science, Technology and Maritime Transport, Alexandria, Egypt

ARTICLE INFO

Article history:
Received 21 July 2022
Received in revised form 8 December 2022
Accepted 23 December 2022
Available online xxxx

Keywords:
Split-source inverter
Predictive control
Virtual synchronous generator
Microgrid

ABSTRACT

Due to high penetration of renewable generation in power systems, and the need to provide the interface between distributed energy resources, the split-source inverter (SSI) provides both the boosting and the conversion capabilities in one single-stage. Also the need for converter-based artificial inertia has become more important. In this paper a model-predictive control (MPC) based on virtual synchronous generator (VSG) algorithm for a parallel-connected three-phase SSI is proposed for conceiving regulation of local voltage and realizing power-sharing of an islanded AC microgrid (MG). A virtual synchronous generator (VSG) is deployed to ensure active-power-sharing and provide inertia-emulation and hence reducing the rate of change of frequency (RoCoF) that results from sudden load change. To accomplish a simple control construction, quick dynamic performance, high stability, and enhanced current limitation, a finite-set MPC (FS-MPC) is used. The analysis and modeling of the proposed technique are presented in detail. A simulation model is used to investigate the proposed system performance.

1. Introduction

The interface between distributed energy resources (DERs) and a common AC bus in an AC MG is provided by voltage source converters (VSCs). Hence, the large-scale penetration of distributed and micro-grid systems based on new energy sources has increased the development of new converter topologies (Meneses et al., 2013). In many application areas, the desired AC voltage is greater than the DC input voltage, requiring the use of conventional two-stage schemes that include a voltage source inverter and a DC boost converter to deliver the energy from the source. A smaller number of power conversion stages with buck–boost capability and lower number of components is provided by the impedance-source inverter (ZSI) (Siwakoti et al., 2015) presented by Peng (2003). However, in order to produce the shoot-through condition, an additional switching states are needed.

The split-source inverter (SSI) proposed by Abdelhakim et al. (2016b) introduces much interesting features compared to the ZSI. A conventional six switches power inverter is employed with three additional diodes provides a single stage power conversion. As a result, the overall voltage stress for all switches is lower than VSI, there are fewer passive elements than ZSI, no additional states when apposed to the ZSIs, and it is designed to boost with a high gain. However, the topology introduces severe commutation losses in the input diodes and unequal current stress on the upper and lower switches. An improvement in the SSI topology was introduced in Lee and Heng (2017) for reducing the high losses of diodes and providing a wide range of AC output voltage in case of buck or boost operation. Furthermore, multilevel topologies as the Flying Capacitor (FC-SSI) (Abdelhakim et al., 2016a) and the Diode Clamped (DC-SSI) (Abdelhakim and Mattavelli, 2016) have been derived from the split-source inverter. Moreover, the SSI system is expanded to the cascaded MLI configuration in a new cascaded multilevel inverter (MLI) topology presented in AbdulSalam et al. (2019). Hence, traditional single-stage and multi-level boosting configurations function more well. For dual three-phase output operation, a split-source nine-switch inverter (NSI) is presented in Dabour et al. (2021) where a reduction of

* Corresponding author.
E-mail addresses: walaa.abouhussein@aiet.edu.eg (W.M. Abou-Hussein), sherif.dabour@gcu.ac.uk (S.M. Dabour), mostafa.hamad@staff.aast.edu (M.S. Hamad), emrashad@f-eng.tanta.edu.eg (E.M. Rashad).

https://doi.org/10.1016/j.egyr.2022.12.075

25% in the number of active switches compared to the dual output inverters is reached using less number of inductors and capacitors in the boosting stage in the DC side.

Some topological modifications have been introduced for the SSI in Abdelhakim et al. (2018), Lee and Heng (2017) and Lee et al. (2019). In Hassan and Shoyama (2018) and Hassan et al. (2020) a discontinuous PWM (DPWM) strategy for reducing the common-mode voltage (CMV) is applied to the SSI. However, the technique does not provide significant CMV reduction and it results in low-frequency ripple on the input current and on the DC-link voltage. In Chaves et al. (2020), two space vector modulation strategies for the SSI was introduced in order to reduce the CMV and hence minimizing the leakage current. The first strategy is based on the selection of specific voltage vectors with similar CMV while the second strategy employs virtual vectors in order to expand the linear operating region of the inverter. A decoupled control strategy has been introduced in Abdelrazek et al. (2017) in which the regulated modified space vector in the synchronous reference frame is employed.

Recently, MPC has been used to control voltage source converters with effectiveness (Rodriguez et al., 2007; Vazquez et al., 2017). Generally, predictive control is employed to predict its future behavior and hence the most appropriate control action can be selected based on an optimality criterion (Kouro et al., 2009; Young et al., 2014). In Borges et al. (2017) there has been introduced a model predictive controller for a three phase split-source inverter.

An AC MG can operate with greater flexibility than a single distributed energy resource (DER) unit since it can manage several VSCs. However, the lack of a rigid voltage supply and inertia, makes controlling an AC MG based on VSC difficult. Grid forming VSCs aim to provide support of voltage and frequency for the islanded mode of operation of AC MGs. Hence, providing an effective control scheme for VSCs is important in order to achieve reliable operation of an islanded AC MG. The DERs are controlled as grid-forming VSCs in the primary control's two main control loops, which are inner loop for regulating local voltage and frequency, and outer loop for manipulating power sharing (Zheng et al., 2020a).

The inner control loop is essential for regulating the whole system. It aims to track the required static and dynamic voltage performance. Cascaded dual-loop linear feedback control has a complex structure, a sluggish dynamic performance, a small control bandwidth, and requires a significant amount of effort to fine-tune the parameters (Dragicevic, 2018). Also, it is difficult for a linear controller to manipulate multi-objective optimization and various constraints of the system (Vazquez et al., 2017; Zheng et al., 2020b; Jongudomkarn et al., 2019).

In order to achieve exact power-sharing when regulating DERs as grid forming converters, droop control with a virtual impedance loop is typically employed for the outer loop of primary control. Nevertheless, the traditional droop control system is unable to give sufficient inertia, leading to a quick RoCoF in the event of disruptions. Furthermore, the stability of the system power-frequency may be significantly impacted by changes in DERs or loads. In D'Arco and Suul (2014), Liu et al. (2016), Beck and Hesse (2007), Rodriguez et al. (2018), Zhong and Weiss (2011), Chen et al. (2019) and Meng et al. (2019), a virtual synchronous generator (VSG) concept is put out with the intention of emulating the inertia of a synchronous generator (SG). A current-controlled VSG method is introduced in Beck and Hesse (2007) and Rodriguez et al. (2018). Nonetheless, because this method only employs a current control loop, it is unable to function in an island state. A voltage-controlled VSG scheme is proposed in Liu et al. (2016) and Zhong and Weiss (2011), which holds up the islanded-mode operation. Nonetheless, it is lacking the current-limiting capability as it only employs a single voltage control loop. Consequently, a cascaded linear control based VSG scheme is put forward in Chen et al. (2019), Meng et al. (2019) and D'Arco et al. (2015), that authorizes both voltage and current control. However, this approach still has the disadvantages of traditional linear control. When compared to linear control, the MPC, in particular the finite-set MPC (FS-MPC), has demonstrated to provide a simple structure, an intrinsic quick transient performance, flexible multi-objective optimization, and the capability to handle constraints (Dragicevic, 2018; Vazquez et al., 2017; Zheng et al., 2020b; Jongudomkarn et al., 2019).

Hence, FS-MPC handle multiple control objectives and constraints by means of only one single cost function (CF). As a consequence, both the cascaded construction and the complexity in adjusting the parameters given by conventional linear control construction can be avoided. In addition, without a modulator, FS-MPC can handle the ideal PWM signals simply, reducing implementation complexities and enabling quick transient responses. Hence, the FS-MPC exhibits the ability to manage VSCs in AC MGs. In Dragicevic (2018), a droop control based FS-MPC scheme is applied to AC MGs for fast and robust operation. However, the control results in a large RoCoF. In Dragicevic (2018), a FS-MPC based on VSG aiming only to enhance the ability of fault-ride though is introduced. However, due to the lack of considering the cross-coupling effect between inductor current and capacitor voltage, ideal steady-state voltage and power sharing response would not occur (de Bosio et al., 2016).

Referring to the mentioned difficulties, a VSG-MPC strategy is proposed in this paper for parallel three-phase connected split-source inverters (SSIs) in islanded AC MGs to optimize conventional primary control with the capability of boosting and inversion in one single stage. Listed below are the contributions we made:

- A SSI is utilized to give both the buck–boost and the inversion capabilities in only one stage with low component ratings, continuous input current, common DC bus and with less number of passive components compared with ZSI and with no need for extra state.
- Employing VSG-MPC achieves improved current-limiting abilities and adaptability to model mismatches which is absent in VSG based linear control.
- The applied VSG-MPC frequency domain performance is compared with that of a linear-control based VSG, demonstrating that utilizing VSG-MPC approach could produce a faster dynamic response and hence improved system stability.
- The proposed system achieves a compact structure, increased transient response and robustness of local voltage, as well as inertia emulation for islanded AC MGs, by combining SSI with FS-MPC and a voltage-controlled VSG.

The structure of this paper is as follows. The modeling of the MG is shown in Section 2. In Section 3, the proposed algorithm of the MPC based VSG for a parallel connected three-phase split-source inverter in an AC MG is detailed. Simulation results are given in Section 4. Finally, the conclusions are provided in Section 5.

2. The system model

A paralleled two-level three-phase split-source inverters supplying an islanded AC microgrid with a LC filter connected to each inverter is shown in Fig. 1 where L_f is the filter-inductance and C_f is the filter-capacitance. The filter dynamic model is specified by (1).

$$\frac{d}{dt}\begin{bmatrix}\bar{i}_f\\ \bar{v}_f\end{bmatrix}=\begin{bmatrix}0 & -\frac{1}{L_f}\\ \frac{1}{c_f} & 0\end{bmatrix}\begin{bmatrix}\bar{i}_f\\ \bar{v}_f\end{bmatrix}+\begin{bmatrix}\frac{1}{L_f}\\ 0\end{bmatrix}\bar{v}_i+\begin{bmatrix}0\\ -\frac{1}{c_f}\end{bmatrix}\bar{i}_o \tag{1}$$

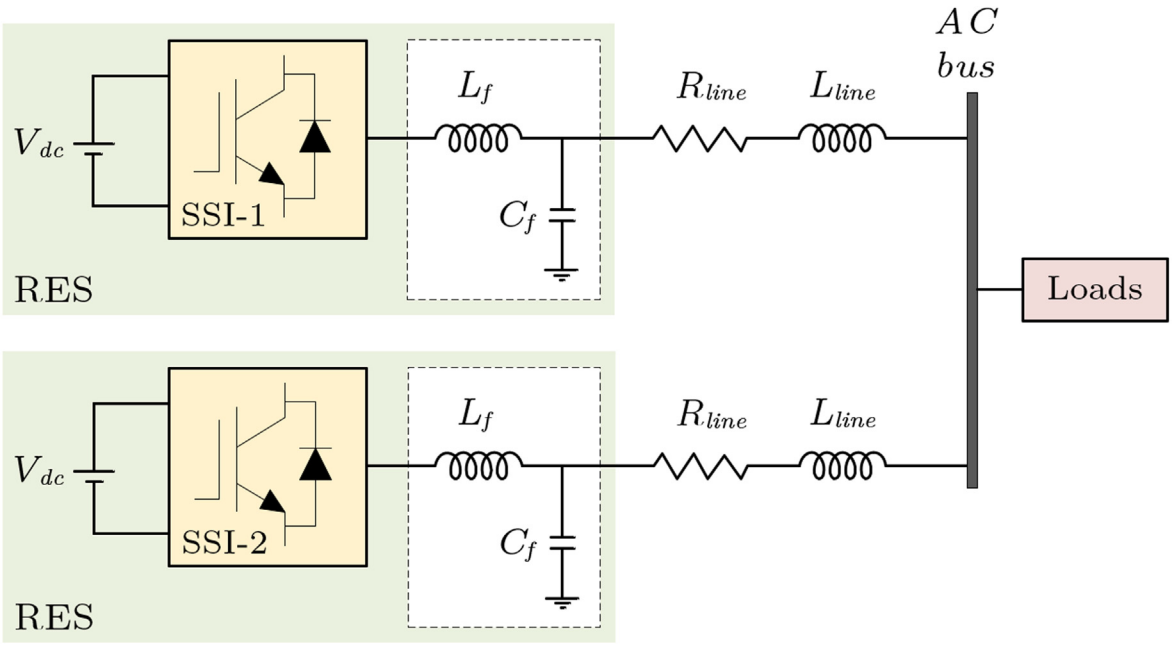

Fig. 1. A paralleled two-level three-phase split-source inverters supplying an islanded AC microgrid.

where

$$x = \begin{bmatrix} \bar{i}_f \\ \bar{v}_f \end{bmatrix} \qquad B = \begin{bmatrix} 1/L_f \\ 0 \end{bmatrix}$$
$$A = \begin{bmatrix} 0 & -1/L_f \\ 1/c_f & 0 \end{bmatrix} \qquad B_d = \begin{bmatrix} 0 \\ -1/c_f \end{bmatrix} \tag{2}$$

The filter-capacitor voltage $\bar{v}_f$ and the filter-inductor current $\bar{i}_f$ are the state variables of the system and they are defined in the $\alpha - \beta$ stationary-reference frame by (3), (4). It can be noticed that the state variables are strongly cross-coupled which would remarkably impact the operation of the system. Also, (5) and (6) defines respectively both the output voltage of the inverter $\bar{v}_i$ and the load current $\bar{i}_o$ in the $\alpha - \beta$ stationary-reference frame.

$$\bar{v}_f = v_{f\alpha} + jv_{f\beta} \tag{3}$$
$$\bar{i}_f = i_{f\alpha} + ji_{f\beta} \tag{4}$$
$$\bar{v}_i = v_{i\alpha} + jv_{i\beta} \tag{5}$$
$$\bar{i}_o = i_{o\alpha} + ji_{o\beta} \tag{6}$$

Table 1 gives the total voltage vectors of the output voltage of the inverter.

3. Proposed MPC based VSG for a three-phase SSI

A three-phase SSI controlled by MPC based VSG is proposed to improve the control of AC microgrids and have the capability to go over the boosting restrictions imposed by VSIs.

3.1. The three-phase two-level split-source inverter (SSI)

Fig. 2 shows a three-phase SSI, with the same bridge as the traditional three-phase VSI having three diodes connected in series with the input DC voltage through one inductor L. In order to charge the inductor, at least one of the lower semiconductor switches S_4, S_6, and S_2 should be turned-on. The capacitor will then be charged from the inductor when at least one of the upper switches S_1,S_3, and S_5 is turned-on.

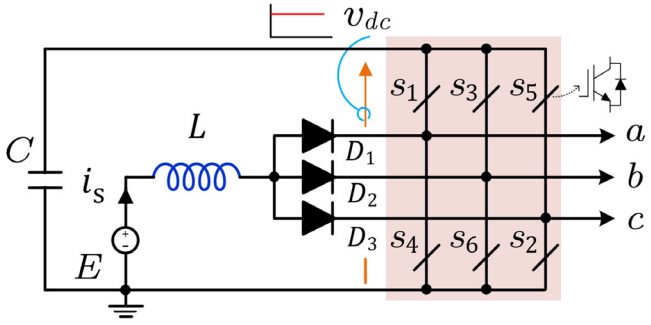

Fig. 2. Three-phase split-source inverter.

Table 1
Switching states and output voltage vectors of The SSI Topology.

Voltage vectors	Switching states $S = [S_1\ S_3\ S_5]$	SSI output voltages $v_i = [v_{i\alpha}\ v_{i\beta}]$
0	[0 0 0]	[0 0]
1	[1 0 0]	$[2V_{dc}/3\ 0]$
2	[1 1 0]	$[V_{dc}/3\ \sqrt{3}V_{dc}/3]$
3	[0 1 0]	$[-V_{dc}/3\ \sqrt{3}V_{dc}/3]$
4	[0 1 1]	$[-2V_{dc}/3\ 0]$
5	[0 0 1]	$[-V_{dc}/3 - \sqrt{3}V_{dc}/3]$
6	[1 0 1]	$[V_{dc}/3 - \sqrt{3}V_{dc}/3]$
7	[1 1 1]	[0]

Fig. 3 shows the block diagram of the proposed VSG-MPC control of a SSI connected to an AC MG. Two main parts are included in the control of the proposed system that are the inner-loop in which FS-MPC is deployed and the outer-loop in which a VSG controller is utilized. Whereas the outer-loop typically realizes active power-sharing and affords virtual inertia assistance for an AC MG in the islanded mode of operation, the inner-loop intends to attain quick dynamic performance and afford enhanced

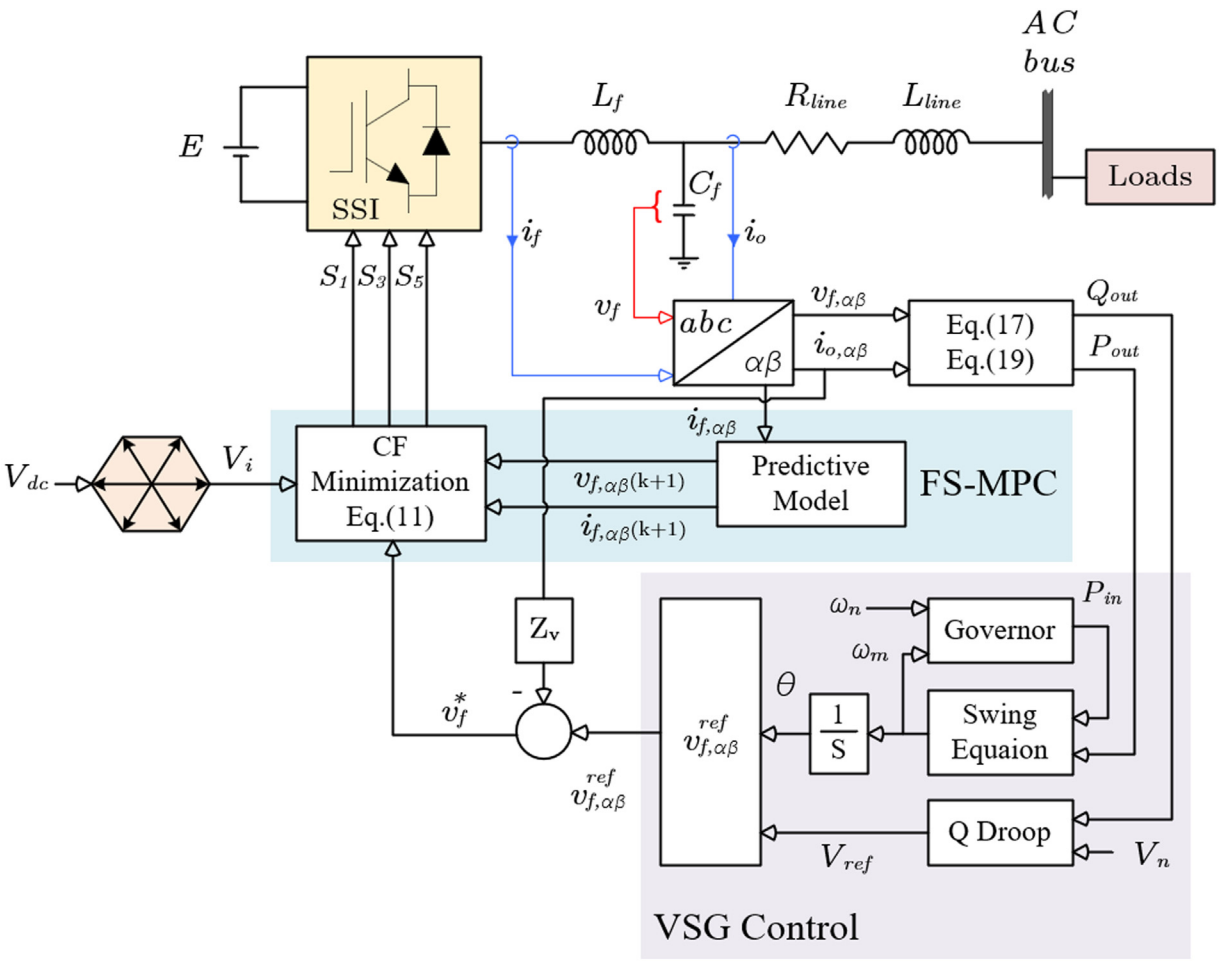

Fig. 3. Block diagram of the proposed VSG-MPC of a SSI.

forceful local voltage. By employing a split-source inverter in the proposed scheme, both the inversion and the boosting stages are provided in one single stage and hence increasing the system efficiency.

3.2. FS-MPC based voltage control

By applying FS-MPC in the inner loop, a fast dynamic response and a robust output voltage can be obtained.

The discrete-time model for a sampling time T_s is given by (7).

$$x(k+1) = A_q x(k) + B_q v_i(k) + B_{dq} i_o(k) \tag{7}$$

where

$$A_q = e^{AT_s} \tag{8}$$

$$B_q = \int_0^{T_s} e^{At}\, B dt \tag{9}$$

$$B_{dq} = \int_0^{T_s} e^{At}\, B_d dt \tag{10}$$

Fig. 4 shows the optimization process based on the FS-MPC algorithm where the value of the state variables, $v_f(k)$ and $i_f(k)$ are measured at the instance k while the reference value of the filter-inductor current $\bar{i}_f^*$ and the reference value of the filter output voltage $\bar{v}_f^*$ are estimated. Then the filter output voltage at the next step $v_f(k+1)$ and the filter-inductor current at the next step $i_f(k+1)$, can be forecasted for every possible voltage vector $\bar{v}_i$ given in Table 1 by using (7).

The cost function (11) is then deployed to select the appropriate voltage vector that guarantees minimizing both the error between the output voltage at the next step $v_f(k+1)$ and its reference v_f^* and also the error between the filter-inductor current at the next step $i_f(k+1)$ and its reference i_f^*. As a result, the appropriate switching state is selected for the next step.

$$\begin{aligned} g = {} & \left(v_{f\alpha}^* - v_{f\alpha}(k+1)\right)^2 + \left(v_{f\beta}^* - v_{f\beta}(k+1)\right)^2 \\ & + \lambda\left(\left(i_{f\alpha}^* - i_{f\alpha}(k+1)\right)^2 + \left(i_{f\beta}^* - i_{f\beta}(k+1)\right)^2\right) + I_{lim} \end{aligned} \tag{11}$$

where, λ is the weighting factor. The filter-capacitor voltage reference $\bar{v}_f^{ref}$ is given by (12) which is then modified to be v_f^* when utilizing a virtual impedance as will be described later.

$$\bar{v}_f^{ref} = V_{ref} cos\left(\omega_{ref}(k)\right) + jV_{ref} sin\left(\omega_{ref}(k)\right) \tag{12}$$

Hence the filter-inductor current is given by

$$\bar{i}_f^* = jC_f\omega_{ref}(k)\,\bar{v}_f^* + \bar{i}_o(k) \tag{13}$$

It could be evidently observed that (13) constitutes the load current, and hence integrating the compensation of the disturbance that could exist in the load current. Accordingly, a robust

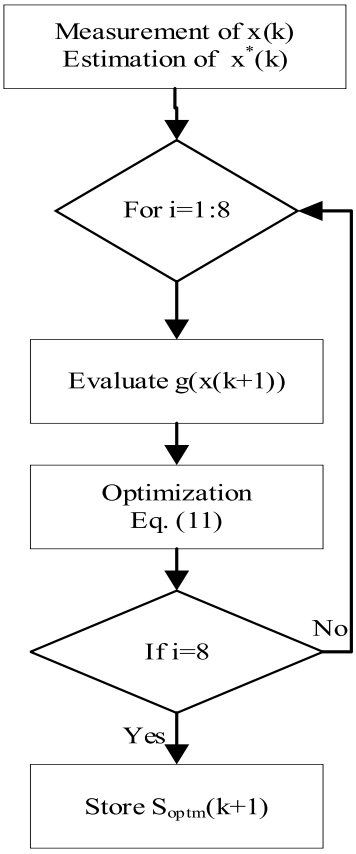

Fig. 4. FS-MPC algorithm.

voltage could be undoubtedly reached even if disturbance in load takes place. A secondary control objective term I_{lim} is included in (11) that can be given by (14) in order to limit the inductor current in case of over-current since FS-MPC permits multi-objectives in control through the cost function.

$$I_{lim} = \begin{cases} \infty, & if \ \left\| i_f(k+1) \right\| > I_{max} \\ 0, & if \ \left\| i_f(k+1) \right\| \leq I_{max} \end{cases} \tag{14}$$

where, I_{max} is the maximum allowable inductor current limit.

FS-MPC can avoid the cascaded construction and the delay of modulation existing in a conventional linear control using just single parameter λ. Thus simple control, easy tuning of the parameters, and fast transient response can be achieved. Furthermore, once the predicted inductor current inclines to exceed I_{max} given by (14), the desired current-limiting capability would be achieved by discarding the related voltage vectors.

3.3. VSG voltage-controller

A VSG voltage-controller is utilized to supply the AC microgrid with virtual inertia. The reference of the output voltage is generated by the VSG controller and then delivered to the MPC controller. Fig. 5 shows the main parts of the VSG controller. It consists of a speed-controller, reactive-power controller and the swing equation part.

The speed-controller is responsible of controlling the active power in case of divergence in frequency depending on the ω-p droop control

$$P_{in} = P_n - k_\omega \left(\omega_m - \omega_n\right) \tag{15}$$

where, k_ω is the coefficient of the $\omega - P$ droop. P_{in} and P_n are the reference of the active power of the VSG and the nominal active power, respectively. ω_m and ω_n are the angular frequency of the VSG and the nominal angular frequency, respectively.

The control of the reactive power is introduced by the Q–V droop control as

$$V_{ref} = V_n - k_q \left(Q_{out} - Q_n\right) \tag{16}$$

where, V_{ref} and V_n are the amplitudes of the voltage reference and nominal voltage, respectively. Q_n is the nominal reactive power. The reactive power Q_{out} is given by

$$Q_{out} = \left(v_{f\beta} i_{o\alpha} - v_{f\alpha} i_{o\beta}\right) \frac{\omega_c}{s + \omega_c} \tag{17}$$

The reference of the output voltage v_f^{ref} is then formed depending on the amplitude of the voltage reference, V_{ref} and the angular frequency, ω_{m} as shown in Fig. 3.

The swing equation is deployed for emulation of the inertia inherited in the rotor of a synchronous generator. It is presented as

$$P_{in} - P_{out} - D\left(\omega_m - \omega_n\right) = J\omega_n d\left(\frac{\omega_m - \omega_n}{dt}\right) \tag{18}$$

where, D is the damping factor and J is the virtual inertia. Any divergence in the frequency would activate J in order to adjust the RoCoF and hence ameliorating the power-frequency stability.

The active output power delivered by the SSI is presented by

$$P_{out} = \left(v_{f\alpha} i_{o\alpha} - v_{f\beta} i_{o\beta}\right) \frac{\omega_c}{s + \omega_c} \tag{19}$$

3.4. Virtual impedance utilization

The accuracy of power sharing is always affected by any difference between the line impedances. Utilizing a virtual impedance allows shaping the output impedance and modifying the reference of the output voltage that is delivered to the inner-loop without affecting the system efficiency.

As a result, the modified voltage reference is given by

$$\overline{v}_f^* = \overline{v}_f^{ref} - Z_v \bar{i}_o \tag{20}$$

where

$$\overline{v}_f^* = v_{f\alpha}^* + j v_{f\beta}^* \tag{21}$$

$$Z_v = R_v + j\omega L_v \tag{22}$$

Z_v is the virtual impedance and R_v is deployed for damping the synchronous resonance.

3.5. Comparative analysis of previous primary control schemes

The need of two stages to boost the DC input voltage in the first stage and invert it to AC in the second stage (Chen and Smedley, 2008) for the interface between renewable energy sources and AC loads suffers from high cost, large size, and large weight of the second stage inherited in the two-stage topologies. Employing ZSI with tank X shape elements as a single stage converter has some limitations such as the extra state in switching which should be shoot-thorough between two switches in one leg or in all legs, inrush current and discontinuous input current. Despite of the several advantages of ZSI, both the large number of passive elements and the switching transformer are considered as a big problem. SSIs has less number of passive components compared with ZSI family. In addition, no need for extra state and it has the same switching states as VSIs with same modulation techniques at normal operation. In addition, the total voltage stress for all

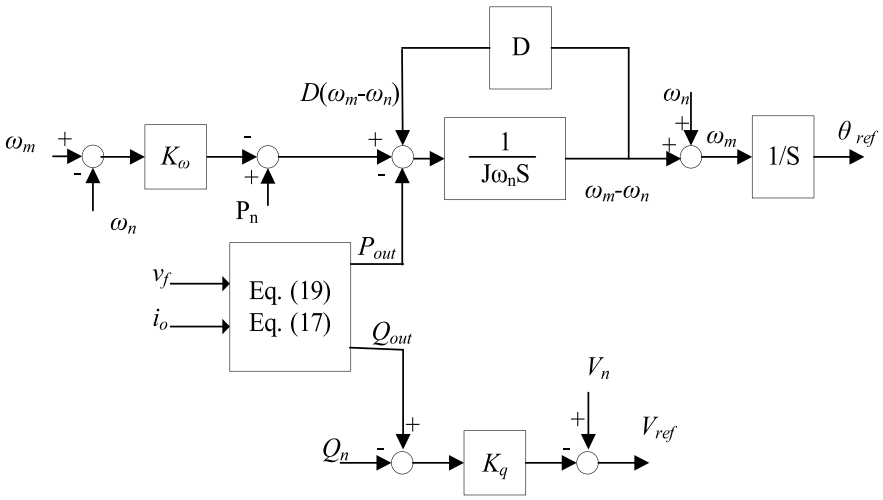

Fig. 5. The scheme of the voltage-controlled VSG.

switches is less than VSI and it has the capability of boosting with high gain.

When comparing the previous control methods, Droop-Linear control cannot offer enough inertia when compared to the VSG-MPC technique. Even while the addition of a specialized leadlag unit makes a modified droop control similar to VSG, it is still not as user-friendly as the straight implementation of VSG (Liu et al., 2016). Moreover, the FS-MPC that is single loop with a single design parameter eliminates the cascaded structure found in traditional linear control schemes that has dual loops with at least three design parameters, which reduces the complexity of implementation and simplifies parameter tuning. Another noteworthy feature of the proposed VSG-MPC is that it can easily handle multi-objective optimization problems that are challenging to resolve by traditional Droop-Linear or VSG-Linear control. Additionally, the presented VSG-MPC does not need measuring the AC-bus frequency, avoiding the phase-locked loop. As opposed to traditional linear-control based systems, the suggested VSG-MPC does not call for a modulator, which results in a shorter computational time and a faster dynamic performance by default. Furthermore, unlike traditional linear-control based methods that have unavoidable over-current ripple, the suggested VSG-MPC may achieve a rigid current-limiting capability. This is due to the distinction in the constraint-handling method between FS-MPC and traditional linear control.

3.6. Stability analysis of the frequency-domain

Due to the nonlinearity of the control approach, the closed-loop frequency domain modeling of the FS-MPC can be established by using a descriptive function (DF). The DF of the FS-MPC provided by (23) can be generated by placing a slight voltage disturbance to the voltage reference $v_{f\alpha}^*$ (Zheng et al., 2020a). The voltage disturbance used is a sinusoidal voltage with a frequency ranging from 100 Hz to 5 kHz and an amplitude of 50 V (Zheng et al., 2020a).

$$DF = \frac{A_m(f_d)}{A_d}\angle\theta_m(f_d) \tag{23}$$

where, A_d and f_d are the amplitude and frequency of the voltage perturbation. By employing discrete Fourier transformation, the output voltage amplitude $A_m(f_d)$ and phase angle $\angle\theta_m(f_d)$ taken at each f_d can be obtained (Quan et al., 2018; Dragičević and Novak, 2019). Consequently, using MATLAB's built-in "tfest" function, an approximated linear transfer function of the DF is given as

$$DF\,(S) = \frac{-1.587e17}{S^4 + 1.79e^4S^3 + 3.83e^7S^2 - 4.3e^{13}S - 1.51e^{17}} \tag{24}$$

The transfer function of the whole VSG-based system is deduced as

$$G_{vsg}\,(S) = G_p(S)G_{SSI}(S)H_{line0}(S) \tag{25}$$

The linear model from active power to electric potential angle is given by

$$G_p\,(S) = \frac{1}{J\omega_n S + D'}\frac{1}{S} \tag{26}$$

where, $D' = D + k_\omega$.

The line resonance has a gain H_{line0} given by (27).

$$H_{line0} = \frac{3}{2}\frac{V_n\,X}{X^2 + R^2} \tag{27}$$

where, $R = R_{line} + R_v$, $X = \omega_n(L_{line} + L_v)$ and $G_{SSI}\,(S) = DF\,(S)$. In low frequency, the SSI part can be omitted as it has unity gain and zero phase shift. As a result, the VSG power regulation part is the presiding part where a pole is given at zero and the other at $-\frac{D'}{J\omega_n}$. Hence, the transfer function of the VSG can be approximated as

$$G_{vsg}\,(S) = G_p\,(S)\,H_{line0} \tag{28}$$

The cross-over frequency is given by

$$\omega_{c0} = \sqrt{\frac{-D'^2 + \sqrt{D'^4 + 4\,(J\omega_n)^2\,{H_{line0}}^2}}{2\,(J\omega_n)^2}} \tag{29}$$

As a result, the conditions that satisfies stability are

$$\begin{cases} \omega_{c0} \le 0.1\omega_n \\ \omega_{c0} \le \dfrac{D'}{J\omega_n} \end{cases}$$

The bode plots of the FS-MPC presented by the DF and the MPC based VSG system are shown in Fig. 6. It can be noticed that the FS-MPC gives rise to a large bandwidth and hence, the dynamic response of voltage is improved. In order to show the dominance of the proposed VSG based FS-MPC system (VSG-MPC) over the VSG based linear control system (VSG-linear) shown in Fig. 7, the bode plots of the proposed VSG-MPC and VSG-Linear control are contrasted in Fig. 6. It is recognizable that the proposed VSG-MPC has a larger magnitude margin than that of conventional VSG-Linear control resulting in enhancement of system stability and

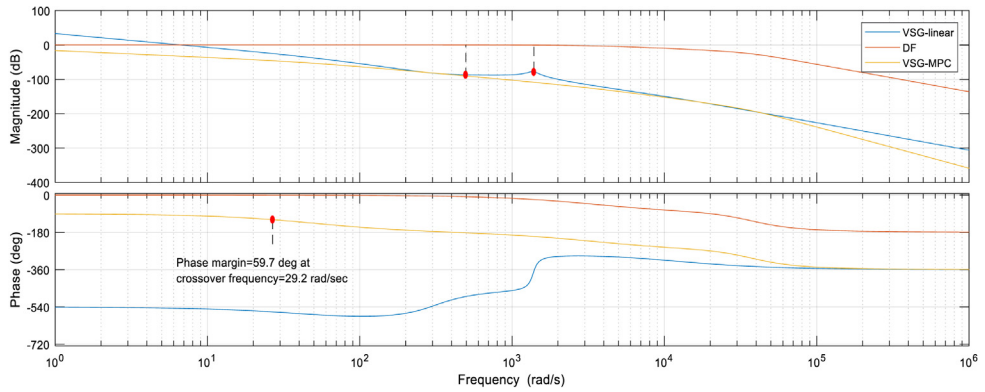

Fig. 6. Block diagram of VSG-linear control of an AC MG.

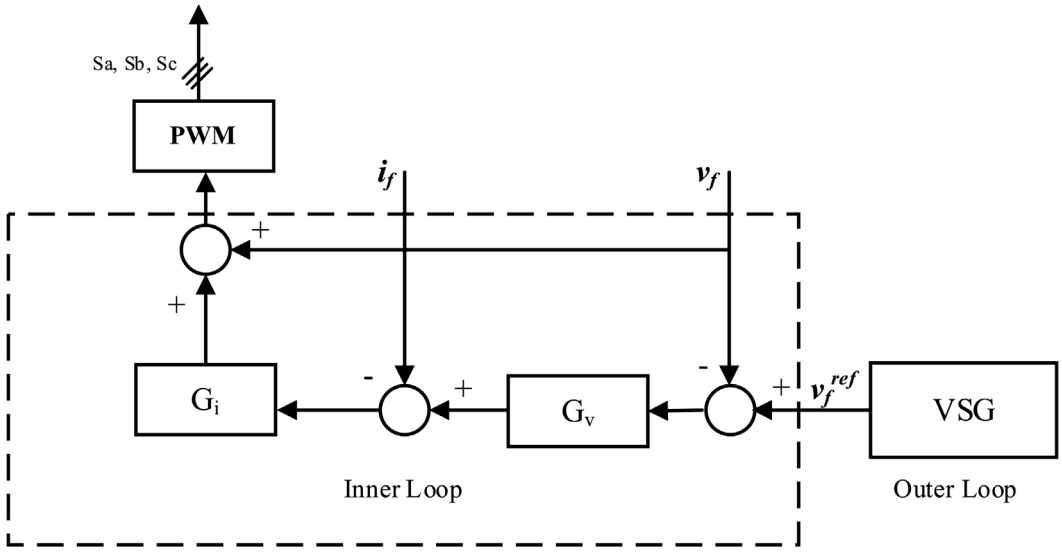

Fig. 7. Comparison of bode plots of conventional VSG-Linear control and proposed VSG-MPC.

robustness. In addition, the crossover frequency ω_{co} for G_{vsg} (S) is 29.2 rad/s which satisfies the conditions for stability that are $\omega_{c0} \leq 0.1\omega_n = 31.4$ rad/s, and $\omega_{c0} \leq \frac{D}{J\omega_n}' = 50$ rad/s.

4. Simulations

The MATLAB/Simulink is used to display the performance of the proposed system given in Fig. 3. However, the proposed approach is limited for low voltage applications due to high switching frequency limitations. Simulation results are based on the parameters provided by Table 2 with a weighting factor $\lambda = 3$ set in the FS-MPC controller which was selected on the basis of an artificial neural network strategy (Dragičević and Novak, 2019). The $\omega -$ P droop coefficient, k_ω is selected by trial and error. The nominal active power P_n and the nominal reactive power Q_n are set to 0 to represent an islanded AC MG autonomously.

4.1. The static and dynamic response

Fig. 8 shows the response of the local voltage and current when a step change in load is applied at time t = 15 s. It can be noticed that the proposed VSG-MPC accomplishes the ability to restore instantaneous voltage. An enhanced steady-state performance with acceptable voltage THD = 0.68% for the proposed system is obtained. This is due to utilizing a dual objective CF that guarantees a fast transient response, a strong and robust system against any load disturbance and hence, achieving the required response of the local voltage.

Fig. 9 shows the steady-state and dynamic performance of the system frequency and the output active power at different values of the weighting factor λ. It can be obviously shown that the system response is affected by the change in λ.

Table 2
System parameters.

Description	Value
Nominal voltage, V_n	200 V
Nominal frequency, f_n	50 Hz
DC bus voltage of VSC, V_{dc}	500 V
DC bus voltage of SSI	400 V
Output LC filter inductor, L_f	2 mH
Output LC filter capacitor, C_f	100 μf
Cut-off frequency of low pass filter, ω_c	100 Hz
Switching frequency, f_{sw}	8 kHz
SSI inductor, L_s	2 mH
SSI capacitor, C	3 mf
ω - P droop coefficient, k_ω	$1/2 * 10^{-3}$
Q - V droop coefficient, k_q	$5 * 10^{-3}$
Moment of virtual inertia, J	0.032 kg m^2
Damping factor, D	0
Virtual resistor, R_v	1 Ω
Virtual inductor, L_v	0.01 H

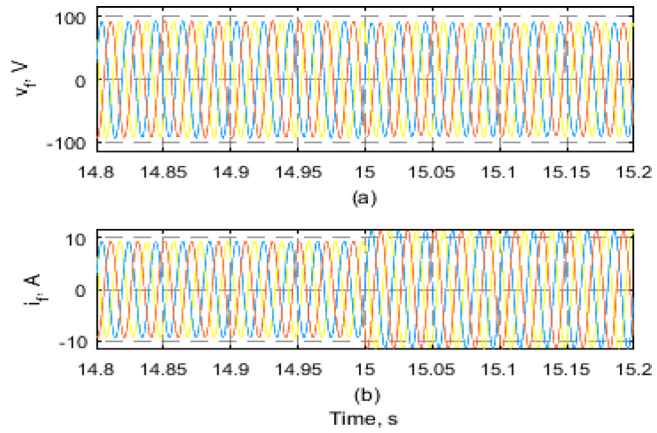

Fig. 8. (a) Local voltage response, v_f and (b) current response, i_f when a step change in load is applied at time t = 15 s.

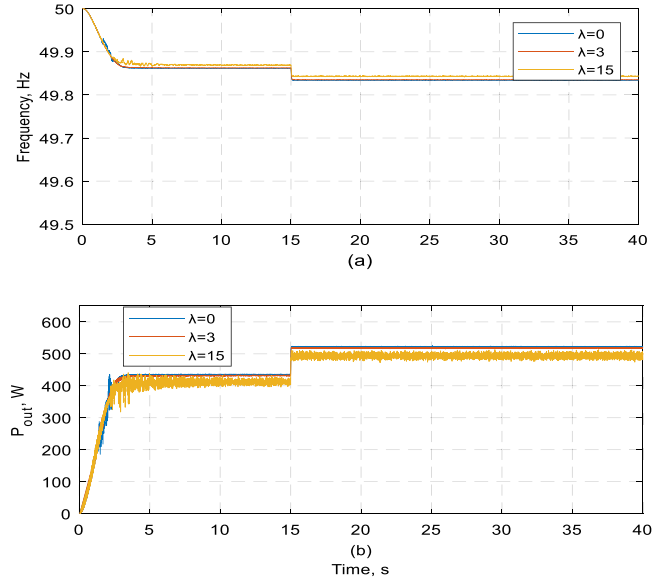

Fig. 9. (a) Frequency response and (b) active power response of the proposed VSG-MPC when a step change in load is applied at time t = 15 s at different values of λ.

Fig. 9 shows that when λ = 0, the FS-MPC is debased into a single objective FS-MPC, which results in a poor transient response. When λ = 3, both the transient and steady-state response are improved. As λ increases, the transient response can be improved but the steady-state response may be deteriorated as can be seen with λ = 15. Hence, a tradeoff in order to balance the static and dynamic response, should be made in the selection of λ.

Fig. 10 shows the response of the system frequency and the active power sharing for the proposed scheme with a step change in load at time t = 15 s. The response ensures that the VSG-based control scheme has a small RoCoF as the settling time t_r = 0.1 s and hence it can increase the system inertia. Also, it can be noticed that a fast transient response for the active-power is reached where t_r = 0.03 s and with a power envelope within 517 W ± 1.5 W.

4.2. Active-power ripples evaluation

The ripples in the active-power of each SSI is evaluated by quantizing the error of the voltage vector of that converter. Fig. 11 shows the active-power sharing performance using the proposed method at different levels of load power. Fig. 11a shows that when the load power is about 430 W, the ripples in the active-power of the proposed method is very modest and have no impact on the transient response. Nevertheless, when the load power is about 80 W as shown in Fig. 11b, the ripple magnitude is slightly large.

In addition, Fig. 12a gives quantization for evaluating the active-power ripples in the steady-state. Moreover, the voltage THD under different values of linear-loads is given in Fig. 12b. The ripples of the active-power P_{out_ripple} is evaluated by

$$P_{out\_ripple} = \sqrt{\frac{1}{N}\sum_{i=1}^{N}\left(P_{out} - P_{out,avg}\right)^2} \tag{30}$$

where, P_{out} is instantaneous active power, $P_{out,avg}$ is mean active power, and N is the point of sampling. It can be noticed from Fig. 12 that under the light-load condition, the proposed VSG-MPC has a low active-power ripple about 1 W and low voltage THD about 0.35%. However, as the load power increases, the active-power ripple shows a slight increase as it is about 1.5 W and also the voltage THD shows a little increase as it is about 0.5%. For much reduction in the ripples of the active-power, (Young et al., 2014; Cortes et al., 2008) introduce some valuable solutions by utilizing the high flexibility of FS-MPC in regulating the switching frequency and including multi-objectives in the cost function. Such solutions are inherently the main advantages of FS-MPC.

4.3. Current-limiting capability evaluation

Fig. 13 shows the current-limiting capability of the system during starting where the limit of the maximum value of the inductor current is I_{max} = 9.8 A. A quick transient response for voltage without overshoot can be observed with the proposed control method. This is due to inclusion of inductor-current limitation in the proposed VSG-MPC of the SSI. Once the predicted inductor-current value inclines to exceed I_{max} defined in (14), the corresponding voltage vector will be directly thrown away and will not be used when evaluating the CF. Hence, the proposed control method guarantees a severe current-limiting capability.

4.4. Model inconsistencies sensibility

Fig. 14 identifies the sensibility of the output voltage to any mismatches in the model resulting from a change of ±50% of nominal C_f and L_f in the controller using proposed VSG-MPC of the SSI by means of a quantitative simulation. A low output-voltage THD is obtained when using the proposed VSG-MPC under an extensive range of parameter variations in filter-inductance and filter-capacitance as depicted in Fig. 14. As a result, the proposed method is less sensitive to model mismatches and hence resulting in a strong robustness.

4.5. Split-source inverter performance

Fig. 15a shows that utilizing the SSI used in the proposed control system results in a DC link capacitor voltage V_{DC} of 520 V from a DC-link voltage of 300 V. In addition, it can be noticed from Fig. 15b that the boosting inductor-current i_{dc} is a continuous current. At steady-state the phase voltage has a peak value of 97.2 V. As a result, the SSI allows both the boosting and inversion capabilities in one single-stage with exact number of active switches and same traditional modulating schemes as in the VSI. Furthermore, a continuously input current is attained.

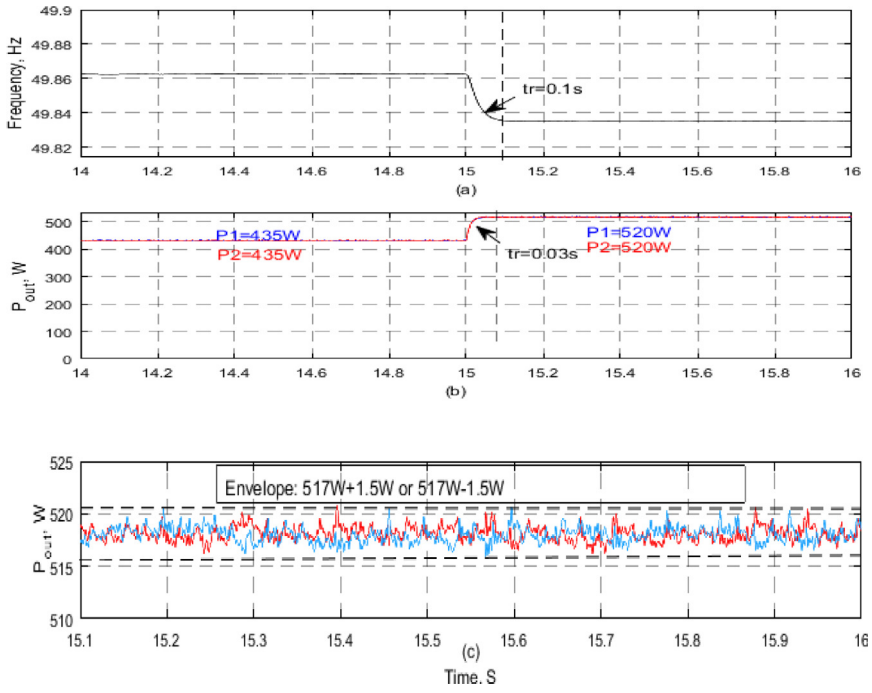

Fig. 10. Simulations: (a) System-frequency, (b) active power sharing and (c) zoomed active-power sharing when a step change in load is applied at time t = 15 s.

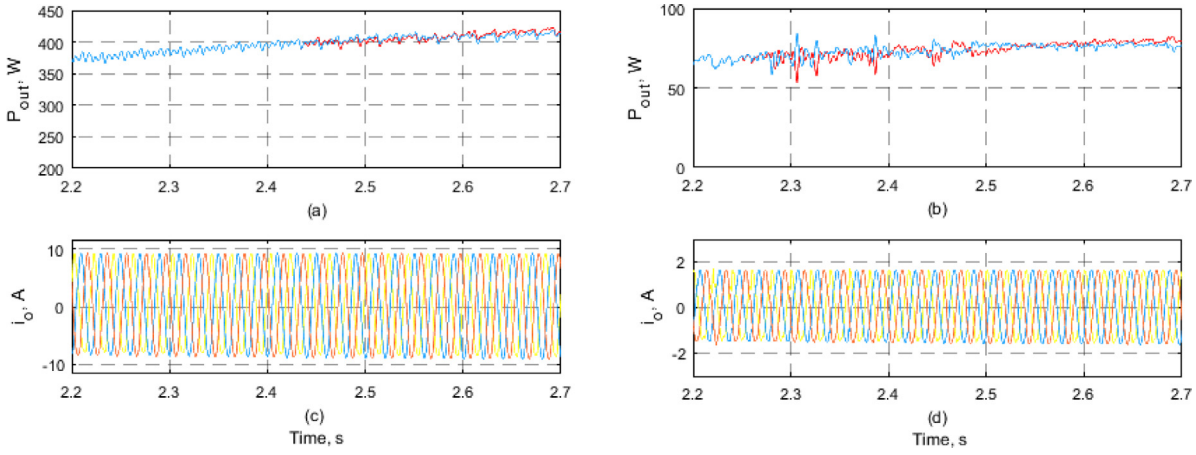

Fig. 11. (a) Active power ripple under a 80 W load, (b) active power ripple under a 430 W load, (c) load current, i_o under a 430 W load and (d) load current under a 80 W load.

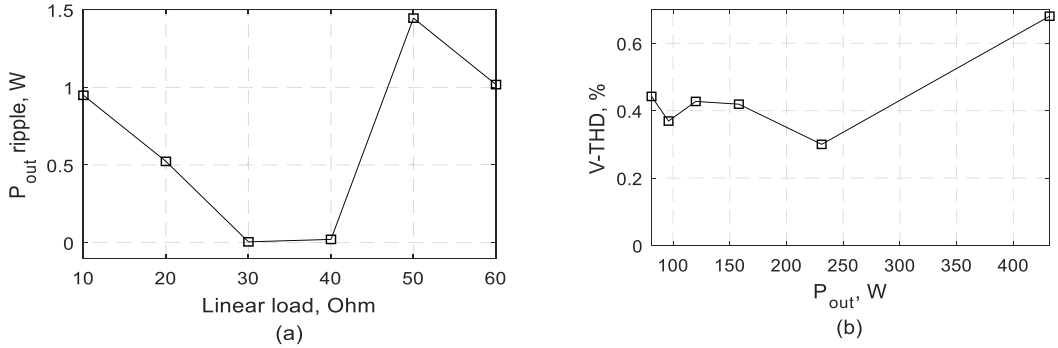

Fig. 12. Evaluation of active power ripples and voltage THD and in steady state. (a) Active power ripples (b) Voltage THD.

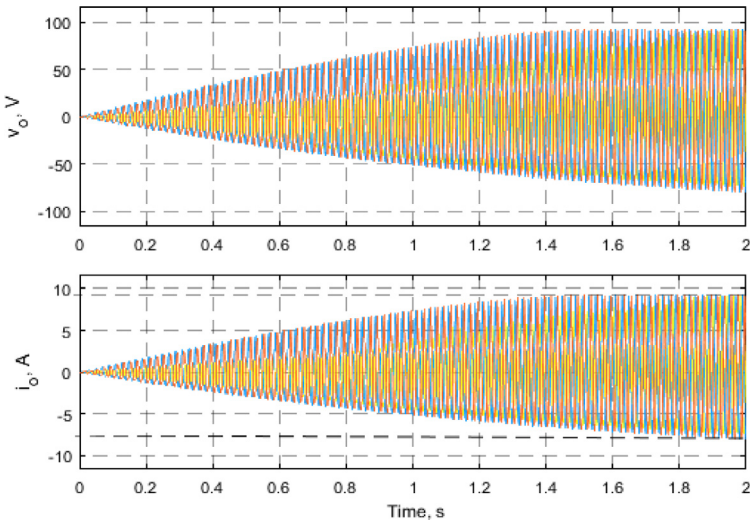

Fig. 13. Current-limiting capability during starting of the system.

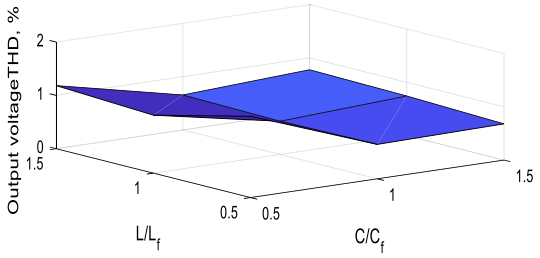

Fig. 14. Output voltage sensibility to model inconsistencies.

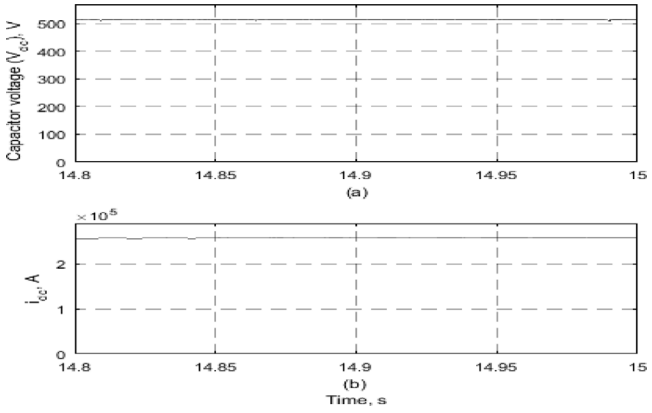

Fig. 15. (a) The DC capacitor voltage, V_{dc} and (b) the boosting inductor current i_{dc}.

5. Conclusion

In this paper, a VSG-MPC scheme for a SSI-based islanded AC MG is proposed to achieve optimization of conventional primary control. A split-source inverter is deployed to get both the inversion and boosting capabilities in one single stage with high gain, less voltage stress, the same modulation techniques as VSI and a less number of passive elements than ZSI. Then, FS-MPC is employed as inner-loop to obtain an output voltage with fast and robust transient response and to provide a severe current limitation. Finally, employing a VSG as an outer-loop control in order to accomplish a precise active power-sharing and to emulate inertia. The analysis of the frequency-domain bode plot ensured that combining a FS-MPC with a VSG control guarantees the enhancement of the system stability. Integrating VSG-MPC with SSI accomplished enhancement of the system stability with both boosting and inversion capabilities in one single stage. The appropriateness and the robustness of the proposed control scheme for AC MGs considering the dynamic and steady-state operations are demonstrated by simulations.

CRediT authorship contribution statement

Walaa M. Abou-Hussein: Conceptualization, Methodology, Software, Writing – original draft. **Sherif M. Dabour:** Supervision, Formal analysis, Writing – review & editing. **Mostafa S. Hamad:** Visualization, Investigation. **Essam M. Rashad:** Supervision, Reviewing and editing.

Declaration of competing interest

The authors declare that they have no known competing financial interests or personal relationships that could have appeared to influence the work reported in this paper.

Data availability

No data was used for the research described in the article.

References

Meneses, D., Blaabjerg, F., García, Ò., Cobos, J., 2013. Review and Comparison of step-up transformerless topologies for photovoltaic ac-module application. IEEE Trans. Power Electron. 28 (6), 2649–2663.

Siwakoti, Y.P., Peng, F.Z., Blaabjerg, F., Loh, P.C., Town, G.E., 2015. Impedance-source networks for electric power conversion part I: A topological review. IEEE Trans. Power Electron. 30 (2), 699–716.

Peng, F.Z., 2003. Z-source inverter. IEEE Trans. Ind. Appl. 39 (2), 504–510.

Abdelhakim, A., Mattavelli, P., Spiazzi, G., 2016b. Threephase split-source inverter (SSI): Analysis and modulation. IEEE Trans. Power Electron. 31 (11), 7451–7461.

Lee, S.S., Heng, Y.E., 2017. Improved single-phase splitsource inverter with hybrid quasi-sinusoidal and constant PWM. IEEE Trans. Ind. Electron. 64 (3), 2024–2031.

Abdelhakim, A., Mattavelli, P., Spiazzi, G., 2016a. Three-phase three-level flying capacitors split-source inverters: Analysis and modulation. IEEE Trans. Ind. Electron. 64 (6), 4571–4580.

Abdelhakim, A., Mattavelli, P., 2016. Analysis of the threelevel diode-clamped split-source inverter. In: 42nd Annual Conference of the IEEE Industrial Electronics Society (IECON'19). pp. 3259–3264.

AbdulSalam, M., Dabour, S.M., Rashad, E.M., 2019. Cascaded multilevel split-source inverters: Analysis and modulation. In: 2019 21st International Middle East Power Systems Conference. MEPCON, pp. 1204–1209.
Dabour, S.M., Abdel-Khalik, A.S., Ahmed, S., Massoud, A., 2021. An optimal PWM technique for dual-output nine-switch boost inverters with minimum passive component count. IEEE Trans. Power Electron. 36 (1), 1065–1079.
Abdelhakim, A., Mattavelli, P., Davari, P., Blaabjerg, F., 2018. Performance evaluation of the single-phase splitsource inverter using an alternative DC-AC configuration. IEEE Trans. Ind. Electron. 65 (1), 363–373.
Lee, S.S., Tan, A.S.T., Ishak, D., Mohd-Mokhtar, R., 2019. Single-phase simplified split-source inverter (S3I) for boost DC-AC power conversion. IEEE Trans. Ind. Electron. 66 (10), 7643–7652.
Hassan, M.S., Shoyama, M., 2018. Common-mode voltage investigation and reduction of split-source inverter. In: 2018 International Conference on Smart Grid (icSmartGrid). pp. 118–122.
Hassan, M.S., Abdelhakim, A., Shoyama, M., Imaoka, J., Dousoky, G.M., 2020. Three-phase split-source inverter-fed PV systems: Analysis and mitigation of common-mode voltage. IEEE Trans. Power Electron. 35 (9), 9824–9838.
Chaves, Brum, D., Grigoletto, F.B., 2020. Space vector modulation techniques for common-mode voltage reduction in three-phase transformerless split-source inverters. Braz. J. Power Electron. 25 (1), 4343–4352.
Abdelrazek, A.A., Mattavelli, P., Boscaino, V., Lullo, G., 2017. Decoupled control scheme of grid-connected split-source inverters. IEEE Trans. Ind. Electron. 64 (8), 6202–6211.
Rodriguez, J., Pontt, J., Silva, C.A., Correa, P., Lezana, P., Cortes, P., Ammann, U., 2007. Predictive current control of a voltage source inverter. IEEE Trans. Ind. Electron. 54 (1), 495–503.
Vazquez, S., Rodriguez, J., Rivera, M., Franquelo, L.G., Norambuena, M., 2017. Model predictive control for power converters and drives: Advances and trends. IEEE Trans. Ind. Electron. 64 (2), 935–947.
Kouro, S., Cortes, P., Vargas, R., Ammann, U., Rodriguez, J., 2009. Model predictive control - a simple and powerful method to control power converters. IEEE Trans. Ind. Electron. 56 (6), 1826–1838.
Young, H.A., Perez, M.A., Rodriguez, J., Abu-Rub, H., 2014. Assessing finite-control-set model predictive control: A comparison with a linear current controller in two-level voltage source inverters. IEEE Ind. Electron. Mag. 8 (1), 44–52.
Borges, D.A., Juliano, Grigoletto, F.B., 2017. Finite set model predictive control of grid connected split-source inverters. In: 2017 Brazilian Power Electronics Conference. COBEP, IEEE, pp. 1–6.
Zheng, C., Dragicevi, T., Blaabjerg, F., 2020a. Model predictive control based virtual inertia emulator for an islanded AC microgrid. IEEE Trans. Ind. Electron. 68 (8), 7167–7177.
Dragicevic, T., 2018. Model predictive control of power converters for robust and fast operation of ac microgrids. IEEE Trans. Power Electron. 33 (7), 6304–6317.
Zheng, C., Dragicevic, T., Blaabjerg, F., 2020b. Current-sensorless finite-set model predictive control for LC-filtered voltage source inverters. IEEE Trans. Power Electron. 35 (1), 1086–1095.
Jongudomkarn, J., Liu, J., Ise, T., 2019. Virtual synchronous generator control with reliable fault ride-through ability: A solution based on finite set model predictive control. IEEE J. Emerg. Sel. Top. Power Electron. 8 (4), 3811–3824.
D'Arco, S., Suul, J.A., 2014. Equivalence of virtual synchronous machines and frequency-droops for converter-based microgrids. IEEE Trans. Smart Grid 5 (1), 394–395.
Liu, J., Miura, Y., Ise, T., 2016. Comparison of dynamic characteristics between virtual synchronous generator and droop control in inverter based distributed generators. IEEE Trans. Power Electron. 31 (5), 3600–3611.
Beck, H.-P., Hesse, R., 2007. Virtual synchronous machine. In: 2007 9th International Conference on Electrical Power Quality and Utilisation. pp. 1–6.
Rodriguez, P., Citro, C., Candela, J.I., Rocabert, J., Luna, A., 2018. Flexible grid connection and islanding of SPC-based PV power converters. IEEE Trans. Ind. Appl. 54 (3), 2690–2702.
Zhong, Q.C., Weiss, G., 2011. Synchronverters: inverters that mimic synchronous generators. IEEE Trans. Ind. Electron. 58 (4), 1259–1267.
Chen, J., Liu, M., O'Donnell, T., 2019. Replacement of synchronous generator by virtual synchronous generator in the conventional power system. In: 2019 IEEE Power & Energy Society General Meeting. PESGM, pp. 1–5.
Meng, X., Liu, J., Liu, Z., 2019. A generalized droop control for grid supporting inverter based on comparison between traditional droop control and virtual synchronous generator control. IEEE Trans. Power Electron. 34 (6), 5416–5438.
D'Arco, S., Suul, J.A., Fosso, O.B., 2015. Automatic tuning of cascaded controllers for power converters using eigenvalue parametric sensitivities. IEEE Trans. Ind. Appl. 51 (2), 1743–1753.
de Bosio, F., Ribeiro, L.A., Freijedo, F.D., Pastorelli, M., Guerrero, J.M., 2016. Effect of state feedback coupling and system delays on the transient performance of stand-alone VSI with LC output filter. IEEE Trans. Ind. Electron. 63 (8), 4909–4918.
Chen, Yang, Smedley, Keyue, 2008. Three-phase boost-type grid-connected inverter. IEEE Trans. Power Electron. 23 (5), 2301–2309.
Quan, X., Dou, X., Wu, Z., Hu, M., Song, H., Huang, A.Q., 2018. A novel dominant dynamic elimination control for voltage-controlled inverter. IEEE Trans. Ind. Electron. 65 (8), 6800–6812.
Dragičević, T., Novak, M., 2019. Weighting factor design in model predictive control of power electronic converters: An artificial neural network approach. IEEE Trans. Ind. Electron. 66 (11), 8870–8880.
Cortes, P., Rodríguez, J., Quevedo, D.E., Silva, C., 2008. Predictive current control strategy with imposed load current spectrum. IEEE Trans. Power Electron. 23 (2), 612–618.